

# Exact Strong-ETH Violating Eigenstates in the Rydberg-blockaded Atom Chain

Cheng-Ju Lin and Olexei I. Motrunich

*Department of Physics and Institute for Quantum Information and Matter,  
California Institute of Technology, Pasadena, CA 91125, USA*

(Dated: June 12, 2022)

A recent experiment in the Rydberg atom chain observed unusual oscillatory quench dynamics with a charge density wave initial state, and theoretical works identified a set of many-body “scar states” in the Hamiltonian as potentially responsible for the atypical dynamics. In the same nonintegrable Hamiltonian, we discover several eigenstates at *infinite temperature* that can be represented exactly as matrix product states with *finite* bond dimension, for both periodic boundary conditions (two exact  $E = 0$  states) and open boundary conditions (two  $E = 0$  states and one each  $E = \pm\sqrt{2}$ ). This discovery explicitly demonstrates violation of strong eigenstate thermalization hypothesis in this model. These states show signatures of translational symmetry breaking with period-2 bond-centered pattern, despite being in 1d at infinite temperature. We show that the nearby many-body scar states with energies  $E \approx \pm 1.33$  and  $E \approx \pm 2.66$  can be well approximated as “quasiparticle excitations” on top of our exact  $E = 0$  states, and propose a quasiparticle explanation of the strong oscillations observed in experiments.

*Introduction.*— Understanding quantum thermalization in isolated systems has attracted a lot of attention recently, due to not only its own fundamental theoretical interest, but also recent developments in cold atom experiments. Eigenstate thermalization hypothesis (ETH) has emerged as a paradigmatic mechanism for quantum thermalization [1, 2]. Loosely speaking, the hypothesis states that for a generic many-body system, it thermalizes at the level of individual eigenstates. Furthermore, the eigenstates at the same energy density will give the same expectation values of “local-enough” observables in the thermodynamic limit. The strong version of ETH requires validity of the above criteria on *every* eigenstate. While an analytical proof is elusive, many numerical studies have provided strong evidences supporting ETH [3–6].

A recent Rydberg cold atom experiment [7] hinted a new scenario, however. The experiment and numerical studies showed that the system can exhibit atypical thermalization behavior if one prepares the initial state as a charge density wave (CDW) state. On the other hand, a uniform tensor product initial state shows the expected thermalization behavior. This is despite the fact that both initial states are at the same energy density. Reference [8] proposed that this phenomenon can be understood from the presence of a set of special eigenstates in the many-body spectrum, dubbed quantum many-body scar states. Further work in Ref. [9] showed numerically that these scar states exhibit nonthermal expectation values for some observables and logarithmic entanglement scaling in subsystem size. In contrast, a typical thermal eigenstate is expected to have volume-law entanglement scaling. Another recent Ref. [10] proposed a framework within the time-dependent variational principle to capture the unusual quench dynamics.

The second known nonintegrable system hosting such subthermal eigenstates at finite energy is the spin-1

Affleck-Lieb-Kennedy-Tasaki (AKLT) model [11]. Reference [12] explicitly constructed families of exact eigenstates in this model. Using formalism of matrix product states (MPS), further Ref. [13] analytically showed that these exact eigenstates with finite energy density have logarithmic entanglement scaling in subsystem size. These papers thus provided the first analytical demonstration of eigenstates that violate the strong ETH.

Remarkably, we have discovered some exact eigenstates with *finite bond dimension* in the Rydberg atom Hamiltonian studied in Refs. [7, 9, 10, 14] at energy density corresponding to *infinite temperature*. Using MPS formalism, we can analytically express these exact eigenstates and study their properties. The existence of the exact MPS description with finite bond dimension shows that the eigenstates have constant entanglement scaling and are hence even more “nonthermal” than the exact states at finite energy density in Refs. [12, 13]. We calculate expectation values of some observables and compare them to predictions from the canonical ensemble. The discrepancies in the thermodynamic limit show the breakdown of the strong-ETH in the Rydberg atom chain. Furthermore, the exact eigenstates break the lattice translation symmetry in one dimension, despite being effectively at infinite temperature. Using “single mode approximation” (SMA) construction on top of our exact eigenstates, we also find good approximations to nearby scar states, thus possibly relating the existence of the scar states to our exact eigenstates.

*Constrained Hilbert space and Hamiltonian.*— The Hilbert space for the Rydberg atom chain has an unusual non-tensor-product structure. Consider Rydberg atoms on a chain with  $L$  sites, and denote  $|0\rangle$  as the atomic ground state and  $|1\rangle$  as the Rydberg excitation. The Rydberg blockade restricts the appearance of two excited states next to each other. That is, the Hilbert space consists of  $2^L$  tensor product states but excluding

states with  $|\dots 11\dots\rangle$  on any two neighboring sites. Despite the lack of tensor product structure, one can still have ETH concept in this constrained Hilbert space [15].

The dynamics of the Rydberg atom chain within this Hilbert space is well described by the so-called PXP model:

$$H = \sum_{j=2}^{L-1} P_{j-1} X_j P_{j+1} + H_1 + H_L, \quad (1)$$

where  $P = |0\rangle\langle 0|$  is the projector to the Rydberg atom ground state and  $X = |0\rangle\langle 1| + |1\rangle\langle 0|$  describes transitions between the ground state and the excited state. For periodic boundary conditions (PBC), we have  $H_1 = P_L X_1 P_2$  and  $H_L = P_{L-1} X_L P_1$ ; while for open boundary conditions (OBC),  $H_1 = X_1 P_2$  and  $H_L = P_{L-1} X_L$ . For PBC, the Hamiltonian has translation symmetry and inversion symmetry, which can be taken to be relative to any site or any bond center. On the other hand, for OBC, the Hamiltonian has only inversion symmetry relative to the midpoint of the system,  $I : j \rightarrow L - j + 1$ . Furthermore, one can define ‘‘particle-hole transformation’’  $C_{\text{ph}} = \prod_j Z_j$ , where  $Z = |1\rangle\langle 1| - |0\rangle\langle 0|$ . This has the property  $C_{\text{ph}} H C_{\text{ph}}^{-1} = -H$ , which guarantees that the spectrum is symmetric around zero energy; moreover, its intertwining with the inversion symmetry implies presence of exponentially many zero-energy eigenstates [9, 16].

The above Hamiltonian, despite its simple appearance, is not trivially solvable due to the constrained structure of the Hilbert space. While its level-spacing statistics indicates its nonintegrability [9], a recent work [14] has suggested that it could be a deformation from some integrable Hamiltonian.

*Exact eigenstates for periodic boundary conditions.*—These eigenstates exist for even number of sites  $L$ , which we assume throughout. The states are expressed using MPS language. We define  $2 \times 3$  and  $3 \times 2$  matrices

$$B^0 = \begin{pmatrix} 1 & 0 & 0 \\ 0 & 1 & 0 \end{pmatrix}, \quad B^1 = \sqrt{2} \begin{pmatrix} 0 & 0 & 0 \\ 1 & 0 & 1 \end{pmatrix}, \quad (2)$$

$$C^0 = \begin{pmatrix} 0 & -1 \\ 1 & 0 \\ 0 & 0 \end{pmatrix}, \quad C^1 = \sqrt{2} \begin{pmatrix} 1 & 0 \\ 0 & 0 \\ -1 & 0 \end{pmatrix}. \quad (3)$$

Two (unnormalized) exact eigenstates in the PBC can be expressed as

$$|\Phi_1\rangle = \sum_{\{\sigma\}} \text{Tr}[B^{\sigma_1} C^{\sigma_2} \dots B^{\sigma_{L-1}} C^{\sigma_L}] |\sigma_1 \dots \sigma_L\rangle, \quad (4)$$

$$|\Phi_2\rangle = \sum_{\{\sigma\}} \text{Tr}[C^{\sigma_1} B^{\sigma_2} \dots C^{\sigma_{L-1}} B^{\sigma_L}] |\sigma_1 \dots \sigma_L\rangle, \quad (5)$$

where  $\sigma_j = 0$  or  $1$  denotes ground or excited state of the Rydberg atom at  $j$ . Note that configurations with  $(\sigma_j \sigma_{j+1}) = (11)$  violating the Hilbert space constraint

are ruled out since  $B^1 C^1 = 0_{2 \times 2}$ ,  $C^1 B^1 = 0_{3 \times 3}$ . We also denote  $L_b = L/2$ , which is the number of two-site blocks.

Verifying  $H|\Phi\rangle = E|\Phi\rangle$  when  $|\Phi\rangle$  is represented as an MPS is in fact not very straightforward. Here, we note that simple calculation by standard MPS techniques gives  $\bar{E} = \langle \Phi_i | H | \Phi_i \rangle / \langle \Phi_i | \Phi_i \rangle = 0$ , while in Supplemental Material [17] we show that  $\langle \Phi_i | (H - E)^2 | \Phi_i \rangle = 0$ , thereby proving  $H|\Phi_i\rangle = 0$ . We also note that since these states are at  $E = 0$ , their effective temperature  $T = \infty$ .

The norm of the states can be easily calculated via the transfer matrix method in MPS, giving us  $\langle \Phi_i | \Phi_i \rangle = 3^{L_b} + 2 + (-1)^{L_b}$ . The two states are not orthogonal and have overlap  $\langle \Phi_1 | \Phi_2 \rangle = 2[(\sqrt{2}-1)^{L_b} + (-1)^{L_b}(\sqrt{2}+1)^{L_b}]$ ; however, they are linearly independent for  $L_b > 3$  (for  $L_b \leq 3$ , we happen to have  $|\Phi_2\rangle = (-1)^{L_b} |\Phi_1\rangle$ ). For  $L_b > 3$ , the states  $|\Phi_{1,2}\rangle$  in fact break the translational symmetry  $T_x$ , while by construction they are invariant under  $T_x^2$ ; furthermore,  $|\Phi_2\rangle = T_x |\Phi_1\rangle$ . One can form states  $|\Phi_{K=0/\pi}\rangle = |\Phi_1\rangle \pm |\Phi_2\rangle$  that carry definite momenta as befits eigenstates of the translationally invariant Hamiltonian; if they were (nearly)-degenerate ground states of a Hamiltonian, the fact that they carry momenta  $0$  and  $\pi$  would be a finite-size signature of the translational symmetry breaking that appears in the thermodynamic limit.

Let us consider in more detail properties of the state  $|\Phi_1\rangle$  (properties of  $|\Phi_2\rangle$  simply follow by translation by one atom). The breaking of the translational symmetry in this state cannot be detected by any one-site observable. This can be seen from the one-site reduced density matrices, which are in fact the same for all sites,  $\rho^{\text{one-site}} = \frac{2}{3}|0\rangle\langle 0| + \frac{1}{3}|1\rangle\langle 1|$  in the thermodynamic limit [17]. It is worth to mention that, at  $T = \infty$ , the Gibbs ensemble predicts average Rydberg excitation number in the thermodynamic limit  $\langle n_j \rangle_{T=\infty} = (1 + \phi^2)^{-1} \approx 0.2764$ , where  $n_j = |1\rangle\langle 1|$  on site  $j$  and  $\phi = (1 + \sqrt{5})/2$  is the golden ratio. The expectation value in our exact zero-energy eigenstate  $\langle \Phi_1 | n_j | \Phi_1 \rangle / \langle \Phi_1 | \Phi_1 \rangle = \frac{1}{3}$  clearly does not satisfy ETH.

On the other hand, two-site observables can detect the translational symmetry breaking, as can be seen from the corresponding reduced density matrices for subsystems  $[1, 2]$  and  $[2, 3]$  in the  $|\Phi_1\rangle$  state:

$$\rho_{[1,2]}^{\text{two-site}} = \frac{1}{3}(|00\rangle\langle 00| + |01\rangle\langle 01| + |10\rangle\langle 10|), \quad (6)$$

$$\rho_{[2,3]}^{\text{two-site}} = \frac{1}{3}(|00\rangle\langle 00| + |01\rangle\langle 01| + |10\rangle\langle 10|) - \frac{1}{9}(|01\rangle\langle 10| + |10\rangle\langle 01|). \quad (7)$$

In particular, we see that  $|0_j 1_{j+1}\rangle \langle 1_j 0_{j+1}| + \text{H.c.}$  has expectation value  $0$  for  $j$  odd and  $-2/9$  for  $j$  even. Note that another common observable in experiment and numerical studies—‘‘domain wall number’’  $P_j P_{j+1}$ —has expectation value  $1/3$  for any  $j$  and hence does not detect the translational symmetry breaking. Interestingly,

the Gibbs ensemble in the thermodynamic limit gives  $\langle P_j P_{j+1} \rangle_{T=\infty} = \phi/(\phi+2) \approx 0.4472$ , which again directly shows the non-ETH behavior of  $|\Phi_1\rangle$ .

We now discuss symmetry properties of the states. Note that for  $L$  even, the inversion  $I$  defined earlier is inversion relative to a bond center, which is not broken in these states (while inversion relative to a site is broken and is not considered further). Under the inversion symmetry,  $I|\Phi_i\rangle = (-1)^{L_b}|\Phi_i\rangle$ . To see this, in the MPS representation, we have  $I|\Phi_1\rangle = \sum_{\{\sigma\}} \text{Tr}[B_I^{\sigma_1} C_I^{\sigma_2} \dots B_I^{\sigma_{L-1}} C_I^{\sigma_L}] |\sigma_1 \dots \sigma_L\rangle$ , where  $B_I^\sigma \equiv [C^\sigma]^T$  and  $C_I^\sigma \equiv [B^\sigma]^T$ . Consider now  $2 \times 2$  matrix  $X_I \equiv i\sigma_y$  and  $3 \times 3$  matrix  $Y_I \equiv \text{diag}(-1, -1, 1)$ . These satisfy  $X_I B_I^\sigma Y_I^{-1} = B^\sigma$  and  $Y_I C_I^\sigma X_I^{-1} = -C^\sigma$  and give us an MPS gauge transformation that proves  $I|\Phi_1\rangle = (-1)^{L_b}|\Phi_1\rangle$ . For  $|\Phi_2\rangle$ , note that since  $I T_x = T_x^{-1} I$  and  $T_x^2 |\Phi_i\rangle = |\Phi_i\rangle$ , we have  $I|\Phi_2\rangle = (-1)^{L_b}|\Phi_2\rangle$  as well.

While  $C_{\text{ph}}$  is not a symmetry of the Hamiltonian, our states are in fact eigenstates of  $C_{\text{ph}}$  with  $C_{\text{ph}}|\Phi_i\rangle = (-1)^{L_b}|\Phi_i\rangle$ . Indeed, in terms of MPS,  $C_{\text{ph}}|\Phi_1\rangle = \sum_{\{\sigma\}} \text{Tr}[B_c^{\sigma_1} C_c^{\sigma_2} \dots B_c^{\sigma_{L-1}} C_c^{\sigma_L}] |\sigma_1 \dots \sigma_L\rangle$ , where  $B_c^0 = -B^0$ ,  $B_c^1 = B^1$ ,  $C_c^0 = -C^0$ , and  $C_c^1 = C^1$ . Consider  $2 \times 2$  matrix  $X_c \equiv \sigma_z$  and  $3 \times 3$  matrix  $Y_c \equiv \text{diag}(-1, 1, -1)$ . Then applying the gauge transformation  $X_c B_c^\sigma Y_c^{-1} = B^\sigma$ ,  $Y_c C_c^\sigma X_c^{-1} = -C^\sigma$  proves  $C|\Phi_1\rangle = (-1)^{L_b}|\Phi_1\rangle$ . For  $|\Phi_2\rangle$ , noting that  $C_{\text{ph}} T_x = T_x C_{\text{ph}}$ , we easily conclude that  $C_{\text{ph}}|\Phi_2\rangle = (-1)^{L_b}|\Phi_2\rangle$ .

*Eigenstates for open boundary conditions.*— We also found exact eigenstates in OBC with the same bulk MPS. Defining “boundary vectors”  $v_1 = (1, 1)^T$  and  $v_2 = (1, -1)^T$ , we can write four exact eigenstates

$$|\Gamma_{\alpha,\beta}\rangle = \sum_{\{\sigma\}} v_\alpha^T B^{\sigma_1} C^{\sigma_2} \dots B^{\sigma_{L-1}} C^{\sigma_L} v_\beta |\sigma_1 \dots \sigma_L\rangle, \quad (8)$$

where  $\alpha, \beta \in \{1, 2\}$ . These states are linearly independent and their squared norms are  $\langle \Gamma_{\alpha,\alpha} | \Gamma_{\alpha,\alpha} \rangle = 2[3^{L_b} + (-1)^{L_b}]$  and  $\langle \Gamma_{1,2} | \Gamma_{1,2} \rangle = \langle \Gamma_{2,1} | \Gamma_{2,1} \rangle = 2[3^{L_b} - (-1)^{L_b}]$ . The eigenenergies are  $E = 0$  for  $|\Gamma_{\alpha,\alpha}\rangle$ ,  $E = \sqrt{2}$  for  $|\Gamma_{1,2}\rangle$ , and  $E = -\sqrt{2}$  for  $|\Gamma_{2,1}\rangle$ . We can prove that the above states are indeed eigenstates by showing that their energy variances are zero [17].

It is interesting to examine the energy density profiles. Figure 1 shows  $\langle X_j \rangle_{\alpha,\beta} \equiv \langle \Gamma_{\alpha,\beta} | X_j | \Gamma_{\alpha,\beta} \rangle / \langle \Gamma_{\alpha,\beta} | \Gamma_{\alpha,\beta} \rangle$  in each state. We can see from the figure (and also from exact expressions in [17]) that there are localized “energy lumps” at the edges of the chain. The profiles decay exponentially into the bulk with decay length  $2 \ln(3)$ . The integrated energy over each lump is  $\sqrt{2}/2$  or  $-\sqrt{2}/2$  depending on the termination. We can thus loosely think about the different terminations as representing different “edge states.”

It is also instructive to consider the action of symmetries on these states. Under the inversion,  $I|\Gamma_{\alpha,\beta}\rangle = \sum_{\{\sigma\}} v_\beta^T B_I^{\sigma_1} C_I^{\sigma_2} \dots B_I^{\sigma_{L-1}} C_I^{\sigma_L} v_\alpha |\sigma_1 \dots \sigma_L\rangle$ . We can now perform the same gauge transformation as in PBC using

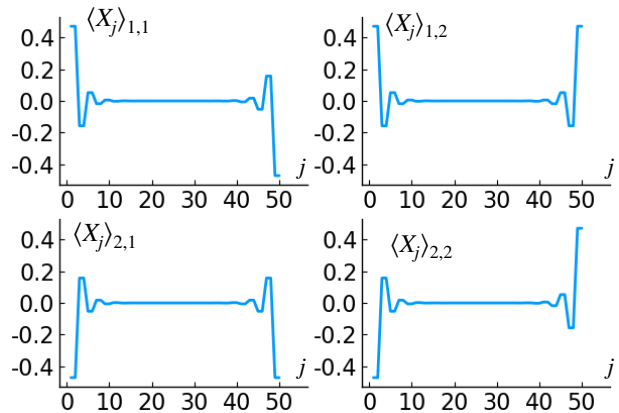


FIG. 1. Energy density profiles  $\langle X_j \rangle_{\alpha,\beta}$  in the four exact eigenstates  $|\Gamma_{\alpha,\beta}\rangle$  in the OBC system of size  $L = 50$ .

matrices  $X_I$  and  $Y_I$ . The boundary vectors transform as  $X_I v_1 = v_2$  and  $X_I v_2 = -v_1$ , and using also  $X_I^{-1} = X_I^T$ , we conclude that  $I|\Gamma_{1,2}\rangle = (-1)^{L_b-1}|\Gamma_{1,2}\rangle$  and  $I|\Gamma_{2,1}\rangle = (-1)^{L_b-1}|\Gamma_{2,1}\rangle$ ; while  $I|\Gamma_{1,1}\rangle = (-1)^{L_b}|\Gamma_{2,2}\rangle$  and  $I|\Gamma_{2,2}\rangle = (-1)^{L_b}|\Gamma_{1,1}\rangle$ . Since  $|\Gamma_{1,1}\rangle$  and  $|\Gamma_{2,2}\rangle$  both have  $E = 0$ , one can form eigenstates  $|\Gamma_{1,1}\rangle \pm |\Gamma_{2,2}\rangle$  with definite inversion quantum numbers  $\pm(-1)^{L_b}$ . We also obtain that  $C_{\text{ph}}|\Gamma_{1,2}\rangle = (-1)^{L_b}|\Gamma_{2,1}\rangle$  and  $C_{\text{ph}}|\Gamma_{1,1}\rangle = (-1)^{L_b}|\Gamma_{2,2}\rangle$ , etc, by employing the same gauge transformation as in PBC with matrices  $X_c$  and  $Y_c$  and noting that the boundary vectors transform as  $X_c v_1 = v_2$  and  $X_c v_2 = v_1$ . The fact that  $|\Gamma_{1,2}\rangle$  and  $|\Gamma_{2,1}\rangle$  are eigenstates of  $I$  means that they can be nondegenerate, which is what we found in exact diagonalization (ED). As expected, these  $E = \pm\sqrt{2}$  eigenstates are related by  $C_{\text{ph}}$ . For the  $E = 0$  exact states, one may wonder if their finite bond dimension is related to the exponential degeneracy of the  $E = 0$  sector. However, this clearly does not apply for the  $E = \pm\sqrt{2}$  states, which suggests more generic character of our findings.

Given the MPS representation of  $|\Gamma_{\alpha,\beta}\rangle$ , we can calculate entanglement for any cut and system size [13, 18]. In the thermodynamic limit, across a cut between  $C_{2b}$  and  $B_{2b+1}$  (bond-dimension  $D = 2$  cut), we find [17] the squared Schmidt values  $1/2, 1/2$ , which gives the von Neumann entanglement entropy  $S_{\text{vN}}^{\text{OBC}, D=2} = \ln 2$ . On the other hand, across a cut between  $B_{2b+1}$  and  $C_{2b+2}$  (bond-dimension  $D = 3$ ), the squared Schmidt values are  $2/3, 1/6, 1/6$ , and  $S_{\text{vN}}^{\text{OBC}, D=3} = -\frac{2}{3} \ln(2/3) - \frac{1}{3} \ln(1/6) \approx 0.868$ .

For the states  $|\Phi_i\rangle$  in PBC and a large subregion, there are two entanglement cuts, and the entanglement entropy in the thermodynamic limit will be sum of the OBC entropies associated with each cut. We can then predict that in the Schrodinger-cat-like states  $|\Phi_{K=0/\pi}\rangle$ ,

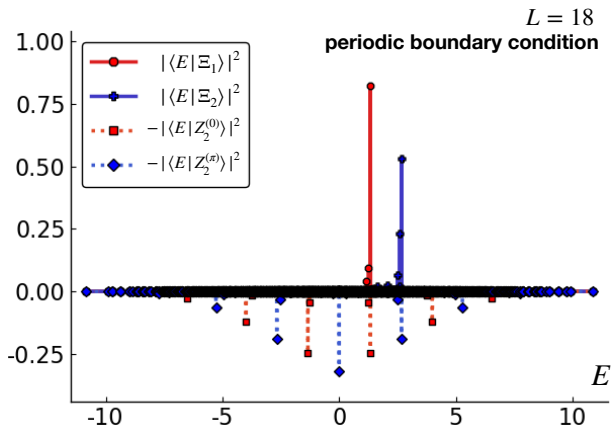


FIG. 2. Overlaps of the SMA wavefunctions with the eigenstates in the PBC system with  $L = 18$ . The  $Z_2$  scar eigenstates are identified through the overlaps with the  $|Z_2^{(0)}\rangle$  or  $|Z_2^{(\pi)}\rangle$  states (for more clarity, we show negatives of these overlaps). Note the high weight of the SMA wavefunctions on the primary scar states.

the entanglement entropy for a large subregion will be  $S_{\text{vN}}^{\text{PBC}} = S_{\text{vN}}^{\text{OBC}, D=2} + S_{\text{vN}}^{\text{OBC}, D=3} + \ln 2 \approx 2.254$ .

*Possible relation to the  $Z_2$  scar states.*— Turner *et al.* [8, 9] identified a set of quantum many-body “scar states” through the overlap of eigenstates  $|E\rangle$  with the CDW states  $|Z_2\rangle = |10\dots 10\rangle$  or  $|Z'_2\rangle = |01\dots 01\rangle$ . The most prominent such scar states have the largest overlap and the smallest entanglement entropy compared to nearby states in the spectrum, but there are also “bands” of weaker scar states close to each primary scar state. The consecutive primary scar states have an almost equal energy separation of  $\approx 1.33$ . The scar states and this frequency were proposed to be responsible for the atypical dynamics showing strong oscillations quenching from the  $|Z_2\rangle$  state.

Since ED finds states with definite momenta, it is convenient to consider states  $|Z_2^{(0,\pi)}\rangle = (|Z_2\rangle \pm |Z'_2\rangle)/\sqrt{2}$ , which carry momenta  $K=0$  and  $K=\pi$  and also have definite inversion quantum numbers  $I=1$  and  $I=-1$  respectively. For  $L_b$  even, the  $Z_2$  scar states at energy  $E \approx 0$  are found to have  $K=0$  and  $I=1$ , while for  $L_b$  odd they have  $K=\pi$  and  $I=-1$ . For a fixed  $L_b$ , both momentum and inversion quantum numbers alternate between these values when going from one primary scar state to the next (and are the same within the band of weaker scar states associated with each primary state). This is also illustrated in Fig. 2.

Turner *et al.* [8, 9] proposed to construct the primary scar states using “forward scattering approximation” starting from the  $Z_2$  state. Here we propose an alternative picture for the scar states near the center of

the many-body spectrum where we start with our exact  $E=0$  states  $|\Phi_i\rangle$  as “mother scar states” and construct nearby scar states by adding “quasiparticle excitations” on top of the mother states.

First, the states  $|\Phi_i\rangle$  have significant overlap with the  $Z_2$  CDW states. We have  $\langle Z_2|\Phi_1\rangle = \langle Z_2|\Phi_2\rangle = (-1)^{L_b} 2^{L_b/2}$ ,  $\langle Z_2^{(\pi)}|\Phi_1\rangle = \langle Z_2^{(\pi)}|\Phi_2\rangle = 2^{L_b/2}$ . We can then calculate overlaps between normalized states with definite momentum and inversion quantum numbers. For  $L_b$  even, we consider  $|\langle Z_2^{(0)}|\Phi_{K=0}\rangle|^2 / \langle \Phi_{K=0}|\Phi_{K=0}\rangle = 8 \cdot 2^{L_b} / \langle \Phi_{K=0}|\Phi_{K=0}\rangle$ , while for  $L_b$  odd, we consider  $|\langle Z_2^{(\pi)}|\Phi_{K=\pi}\rangle|^2 / \langle \Phi_{K=\pi}|\Phi_{K=\pi}\rangle = 8 \cdot 2^{L_b} / \langle \Phi_{K=\pi}|\Phi_{K=\pi}\rangle$ , where  $\langle \Phi_{K=0(\pi)}|\Phi_{K=0(\pi)}\rangle = 2[3^{L_b} + 2 + (-1)^{L_b}] \pm 4[(\sqrt{2}-1)^{L_b} + (-1)^{L_b}(\sqrt{2}+1)^{L_b}]$ . While the overlaps decay exponentially, they are comparable to the corresponding overlaps for the ED scar states at finite size. For example, at  $L=18$ , we have  $|\langle Z_2^{(\pi)}|\Phi_{K=\pi}\rangle|^2 / \langle \Phi_{K=\pi}|\Phi_{K=\pi}\rangle \approx 0.081$ . While this is smaller than the corresponding overlaps for the nearby ED scar states in Fig. 2, it is encouraging that our exact states can capture the  $L_b$  dependence of the momentum and inversion quantum numbers of the  $E=0$   $Z_2$  scar states. Furthermore, we are naturally led to other scar states that have no overlap with the  $Z_2$  states, such as  $|\Phi_{K=0}\rangle$  for  $L_b$  odd and  $|\Phi_{K=\pi}\rangle$  for  $L_b$  even, as well as their nonzero energy descendants.

Turning to the scar states at nonzero energy, we propose to view these as “quasiparticle excitations” on top of the exact  $E=0$  states. More precisely, we construct variational wavefunctions using SMA [19, 20] on top of our exact  $|\Phi_i\rangle$  states, which resembles construction of quasiparticles on top of ground states.

The first variational wavefunction we propose to approximate the first  $E \neq 0$  primary scar state is  $|\Xi_1\rangle = (|M\rangle - (-1)^{L_b} T_x |M\rangle) / \xi_1$ , where

$$|M\rangle = \sum_{\sigma_1}^{L_b} \text{Tr}[B^{\sigma_1} C^{\sigma_2} \dots M^{\sigma_{2b-1} \sigma_{2b}} \dots B^{\sigma_{L-1}} C^{\sigma_L}] |\sigma_1 \dots \sigma_L\rangle, \quad (9)$$

and  $\xi_1$  is the normalization factor,  $\langle \Xi_1|\Xi_1\rangle = 1$ . The matrices

$$M^{00} = \begin{pmatrix} 1 & 0 \\ 0 & 1 \end{pmatrix}, \quad M^{01} = \begin{pmatrix} \mu_1 & 0 \\ \mu_2 & 0 \end{pmatrix}, \quad M^{10} = \begin{pmatrix} 0 & 0 \\ -\mu_2 & \mu_1 \end{pmatrix}$$

are chosen such that the wavefunction satisfies the Rydberg-blockaded constraint and  $I|M\rangle = (-1)^{L_b-1}|M\rangle$ , hence  $I|\Xi_1\rangle = (-1)^{L_b-1}|\Xi_1\rangle$ . We also choose the translation quantum number of  $|\Xi_1\rangle$  to be  $(-1)^{L_b-1}$ , which is in the symmetry sector of the first  $E \neq 0$  scar state overlapping with the  $Z_2$  CDW [21]. To make  $|\Xi_1\rangle$  as close to an eigenstate as possible, we minimize the energy variance  $f_1(\mu_1, \mu_2) = \langle \Xi_1|H^2|\Xi_1\rangle - \langle \Xi_1|H|\Xi_1\rangle^2$  at fixed  $L$ . At  $L=18$ , we find optimal parameters  $\mu_1 = 1.08457$  and  $\mu_2 = -0.6318$ , which give the energy variance  $f_1 = 0.025$  and average energy  $\langle \Xi_1|H|\Xi_1\rangle = 1.32$ . Remarkably, the

optimized state has over 82% overlap with the primary  $Z_2$  scar state at  $E \approx 1.34$  found in ED, as shown in Fig. 2. Using the gauge transformation  $X_c, Y_c$  from our discussion of the action of  $\mathcal{C}_{\text{ph}}$  on  $|\Phi_1\rangle$ , it is easy to check that  $\mu'_1 = -\mu_1, \mu'_2 = \mu_2$  gives  $|\Xi'_1\rangle = (-1)^{L_b-1}\mathcal{C}_{\text{ph}}|\Xi_1\rangle$ , which will capture the scar state with  $E \approx -1.34$ .

The second SMA-type variational wavefunction we consider is  $|\Xi_2\rangle = (|N\rangle + (-1)^{L_b}T_x|N\rangle)/\xi_2$ , where  $|N\rangle$  is defined similar to Eq. (9) but replacing the matrices  $M$  with  $N$  ( $\xi_2$  is the normalization factor). The matrices

$$N^{00} = \begin{pmatrix} \nu & \sqrt{2} \\ -\sqrt{2} & -\nu \end{pmatrix}, \quad N^{01} = \begin{pmatrix} 1 & 0 \\ 0 & 0 \end{pmatrix}, \quad N^{10} = \begin{pmatrix} 0 & 0 \\ 0 & -1 \end{pmatrix}$$

are chosen such that the wavefunction satisfies the Rydberg-blockaded constraint,  $I|N\rangle = (-1)^{L_b}|N\rangle$ , and  $|N\rangle$  is orthogonal to  $|\Phi_1\rangle$ . (More precisely,  $|N\rangle$  is orthogonal for  $L_b$  even and has exponentially small overlap for  $L_b$  odd). The momentum quantum number of  $|\Xi_2\rangle$  is constructed to be the same as the second primary scar state. We again find the optimal parameters by minimizing the energy variance  $f_2(\nu) = \langle \Xi_2|H^2|\Xi_2\rangle - \langle \Xi_2|H|\Xi_2\rangle^2$ , finding  $\nu = 2.381$  at  $L = 18$  and giving us  $f_2 = 0.33$  and  $\langle \Xi_2|H|\Xi_2\rangle = 2.47$ . The state has over 53% overlap with the primary scar state with  $E \approx 2.67$ , as shown in Fig. 2. Using the gauge transformation  $X_c, Y_c$ , we can see that  $\nu' = -\nu$  gives the state  $|\Xi'_2\rangle = (-1)^{L_b}\mathcal{C}_{\text{ph}}|\Xi_2\rangle$  with the negative energy.

We now discuss these results.  $|\Xi_1\rangle$  and  $|\Xi'_1\rangle$  can be viewed as representing “elementary quasiparticles” with energies  $\epsilon_+ \approx 1.34$  and  $\epsilon_- = -\epsilon_+$ ; these particles also carry inversion quantum number  $-1$ . It is then natural to expect strong oscillations with frequency given by  $\epsilon_+$  in observables that can flip the inversion quantum number. (Observables in experiment and numerical studies that do not change the inversion quantum number will show twice the frequency.) Indeed, even though the overlaps of the  $Z_2$  initial state with the primary scar states decrease exponentially with system size, the “quasiparticle creation operators” can also act on many more states, always “adding” roughly the quasiparticle excitation energy. This argument resembles the quasiparticle explanation [22] of strong oscillations in the “weak thermalization” regime discovered in a nonintegrable model in Ref. [23], where the initial state happened to be near the ground state. The differences here are that the initial  $Z_2$  state is at  $T = \infty$  but is “close” to our special eigenstates  $|\Phi_i\rangle$ , and that the quasiparticles here can carry both positive and negative energies.

By repeated application of the SMA construction that gave us the  $|\Xi_1\rangle$  and  $|\Xi'_1\rangle$  states, we also expect additional states with energies  $E \approx (n_+ - n_-)\epsilon_+$ ,  $n_+, n_- \in \mathbb{N}$ . Interestingly, the same energy  $m\epsilon_+$  can be obtained in multiple ways, which may explain the bands of weaker scar states visible near the primary states in Ref. [9].

We also note that  $|\Xi_2\rangle$  can be viewed as using a different “quasiparticle” but trying to capture an excitation

potentially with two  $\epsilon_+$  quasiparticles. This may be the reason why the quality of  $|\Xi_2\rangle$  is worse than the quality of  $|\Xi_1\rangle$ . On the other hand, it is likely that  $|\Xi_2\rangle$  has less entanglement and is a more special state compared to two free quasiparticles, which may be a useful feature of this construction.

Finally, we note that the presented simple “bond-dimension-2” SMA wavefunctions cover cases where we would replace one  $B$  site or one  $C$  site with an “excitation,” or “excite” two consecutive  $B_{2b-1}, C_{2b}$  matrices. One can also consider exciting two consecutive  $C_{2b}, B_{2b+1}$  matrices, which would lead to new “bond-dimension-3” SMA wavefunctions with more variational parameters. Our quick study of such new wavefunctions shows that they can reproduce the same first and second primary scar states with even higher fidelity, but since the improvement is only quantitative and the states have more parameters, we focused on the bond-dimension-2 SMA.

*Conclusion.*- In this work, we presented exact eigenstates in the Rydberg-blockaded atom chain at finite energy-density corresponding to  $T = \infty$  that explicitly violate the strong-ETH. Our exact states have constant entanglement scaling in subsystem size. In contrast, previous works have found logarithmic entanglement scaling numerically on the scar states in the same model and analytically on the exact states in the AKLT model. Our exact states show translation symmetry breaking, which implies two-fold degeneracy in PBC. We also found exact eigenstates in OBC, which have the same bulk as in PBC and can have different edge terminations leading to different eigenenergies, including nondegenerate energies.

This discovery paves a possible way to understand other scar states at nearby energies. By constructing SMA quasiparticles on top of the exact states, we can capture the first and second nearby primary scar states with high fidelity. Many detailed questions remain to be explored. The possibility of capturing other primary scar states as well as bands of weaker scar states by constructing multiple quasiparticle “excitations” is worth to corroborate. Also, our SMA states have finite entanglement entropy but are only approximations. Could there be a convergent finite-entanglement improvement on the SMA states (or perhaps even some new exact constructions), or do the exact primary scar states have entanglement entropy growing unbounded with the system size as proposed in Ref. [9]? In the latter case, could the SMA states be still capturing some precise information about the bands associated with the primary scar states? We leave these questions for future work.

*Acknowledgments.*- We thank V. Albert, M. Endres, B. Roberts, B. Timar, and C. White for valuable discussions. This work was supported by NSF through grant DMR-1619696, and also by the Institute for Quantum Information and Matter, an NSF Physics Frontiers Center, with support of the Gordon and Betty Moore Foundation.

- 
- [1] J. M. Deutsch, *Phys. Rev. A* **43**, 2046 (1991).
- [2] M. Srednicki, *Phys. Rev. E* **50**, 888 (1994).
- [3] M. Rigol, V. Dunjko, V. Yurovsky, and M. Olshanii, *Phys. Rev. Lett.* **98**, 050405 (2007).
- [4] M. Rigol, V. Dunjko, and M. Olshanii, *Nature* **452**, 854 (2008).
- [5] H. Kim, T. N. Ikeda, and D. A. Huse, *Phys. Rev. E* **90**, 052105 (2014).
- [6] J. R. Garrison and T. Grover, *Phys. Rev. X* **8**, 021026 (2018).
- [7] H. Bernien, S. Schwartz, A. Keesling, H. Levine, A. Omran, H. Pichler, S. Choi, A. S. Zibrov, M. Endres, M. Greiner, V. Vuletić, and M. D. Lukin, *Nature* **551**, 579 (2017).
- [8] C. J. Turner, A. A. Michailidis, D. A. Abanin, M. Serbyn, and Z. Papić, *Nat. Phys.* **14**, 745 (2018).
- [9] C. J. Turner, A. A. Michailidis, D. A. Abanin, M. Serbyn, and Z. Papić, arXiv:1806.10933 (2018), arXiv:1806.10933.
- [10] W. W. Ho, S. Choi, H. Pichler, and M. D. Lukin, arXiv:1807.01815 (2018), arXiv:1807.01815.
- [11] I. Affleck, T. Kennedy, E. H. Lieb, and H. Tasaki, *Phys. Rev. Lett.* **59**, 799 (1987).
- [12] S. Moudgalya, S. Rachel, B. A. Bernevig, and N. Regnault, arXiv:1708.05021 (2017), arXiv:1708.05021.
- [13] S. Moudgalya, N. Regnault, and B. A. Bernevig, arXiv:1806.09624 (2018), arXiv:1806.09624.
- [14] V. Khemani, C. R. Laumann, and A. Chandran, arXiv:1807.02108 (2018), arXiv:1807.02108.
- [15] A. Chandran, M. D. Schulz, and F. J. Burnell, *Phys. Rev. B* **94**, 235122 (2016).
- [16] M. Schechter and T. Iadecola, *Phys. Rev. B* **98**, 035139 (2018).
- [17] See Supplemental Material.
- [18] J. I. Cirac, D. Poilblanc, N. Schuch, and F. Verstraete, *Phys. Rev. B* **83**, 245134 (2011).
- [19] J. Haegeman, B. Pirvu, D. J. Weir, J. I. Cirac, T. J. Osborne, H. Verschelde, and F. Verstraete, *Phys. Rev. B* **85**, 100408 (2012).
- [20] J. Haegeman, S. Michalakis, B. Nachtergaele, T. J. Osborne, N. Schuch, and F. Verstraete, *Phys. Rev. Lett.* **111**, 080401 (2013).
- [21] Choosing combination  $\sim |M\rangle + (-1)^{L_b} T|M\rangle$  instead gives a state with translation quantum number  $(-1)^{L_b}$  and inversion quantum number  $(-1)^{L_b-1}$ , which does not overlap with the  $Z_2$  CDW state but is an interesting scar state as well. Curiously, at  $L = 12$  (or  $L_b = 6$ ), such variational wavefunctions with parameters  $\mu_1 = \pm\sqrt{2}$  and  $\mu_2 = -\sqrt{2}$  are eigenstates with energies  $E = \pm\sqrt{2}$ .
- [22] C.-J. Lin and O. I. Motrunich, *Phys. Rev. A* **95**, 023621 (2017).
- [23] M. C. Bañuls, J. I. Cirac, and M. B. Hastings, *Phys. Rev. Lett.* **106**, 050405 (2011).

**Supplemental Material for: Exact Strong-ETH Violating Eigenstates in the Rydberg-blockaded Atom Chain**

**Proof of exact eigenstates in PBC**

Here we prove that  $H|\Phi_1\rangle = 0$  by showing that the norm of the state  $H|\Phi_1\rangle$  is zero. To prove this, it is easier to work in the blocked reformulation of the Hamiltonian: We block two sites  $2b - 1, 2b$  into one “block-site”, with allowed block states  $(00)$ ,  $(10)$ , and  $(01)$  denoted as  $O$ ,  $L$ , and  $R$  respectively; the Rydberg constraint further disallows configurations with  $RL$  on consecutive blocks. The number of blocks is  $L_b = L/2$ , and recall that throughout we assume that  $L$  is even. In the blocked representation, the Hamiltonian can be written as a sum of two-body terms:

$$H = \sum_{b=1}^{L_b} h_{b,b+1}, \quad h_{b,b+1} = (|R\rangle\langle O| + |O\rangle\langle R|)_b \otimes (I - |L\rangle\langle L|)_{b+1} + (I - |R\rangle\langle R|)_b \otimes (|L\rangle\langle O| + |O\rangle\langle L|)_{b+1}. \quad (10)$$

The state  $|\Phi_1\rangle$  can be written in the blocked representation as an MPS of bond dimension 2, namely

$$|\Phi_1\rangle = \sum_{\{s\}} \text{Tr}[A^{s_1} \dots A^{s_{L_b}}] |s_1 \dots s_{L_b}\rangle, \quad (11)$$

where we have introduced blocked matrices  $A^{(\sigma_1\sigma_2)} = B^{\sigma_1}C^{\sigma_2}$ . Explicitly,

$$A^O = \begin{pmatrix} 0 & -1 \\ 1 & 0 \end{pmatrix}, \quad A^R = \begin{pmatrix} \sqrt{2} & 0 \\ 0 & 0 \end{pmatrix}, \quad A^L = \begin{pmatrix} 0 & 0 \\ 0 & -\sqrt{2} \end{pmatrix}. \quad (12)$$

One can easily check that  $A^R A^L = 0$ , so the state satisfies the Rydberg constraint between the blocks. (Interestingly, these matrices also satisfy  $A^L A^R = 0$ , so this state also disallows  $LR$  on consecutive blocks.)

Calculations with the MPS state heavily use the associated transfer matrix defined as

$$E_A = \sum_s (A^s)^* \otimes A^s = \begin{pmatrix} 2 & 0 & 0 & 1 \\ 0 & 0 & -1 & 0 \\ 0 & -1 & 0 & 0 \\ 1 & 0 & 0 & 2 \end{pmatrix}, \quad (13)$$

and we immediately get

$$E_A^m = \frac{1}{2} \begin{pmatrix} 1 + 3^m & 0 & 0 & -1 + 3^m \\ 0 & 1 + (-1)^m & -1 + (-1)^m & 0 \\ 0 & -1 + (-1)^m & 1 + (-1)^m & 0 \\ -1 + 3^m & 0 & 0 & 1 + 3^m \end{pmatrix}. \quad (14)$$

The norm of the state is  $\langle \Phi_1 | \Phi_1 \rangle = \text{Tr}[E_A^{L_b}] = 3^{L_b} + 2 + (-1)^{L_b}$ .

We first examine how the genuinely two-body part of the Hamiltonian term  $h_{b,b+1}$ , namely  $h_{b,b+1}^{(2)} \equiv -(|R\rangle\langle O| + |O\rangle\langle R|)_b \otimes (|L\rangle\langle L|)_{b+1} - (|R\rangle\langle R|)_b \otimes (|L\rangle\langle O| + |O\rangle\langle L|)_{b+1}$  operates on  $|\Phi_1\rangle$ . The special property  $A^R A^L = 0$  leaves us only the part  $-(|R\rangle\langle O|)_b \otimes (|L\rangle\langle L|)_{b+1} - (|R\rangle\langle R|)_b \otimes (|L\rangle\langle O|)_{b+1}$ . It is easy to check that the matrices also satisfy  $A^O A^L + A^R A^O = 0$ , and hence we conclude that  $h_{b,b+1}^{(2)} |\Phi_1\rangle = 0$ .

Consider now the action of one-body terms association with block  $b$ :

$$\left( |R\rangle\langle O| + |O\rangle\langle R| + |L\rangle\langle O| + |O\rangle\langle L| \right)_b |\Phi_1\rangle = \sum_{\{s\}} \text{Tr}[A^{s_1} \dots F^{s_b} \dots A^{s_{L_b}}] |s_1 \dots s_{L_b}\rangle, \quad (15)$$

where

$$F^O = \begin{pmatrix} \sqrt{2} & 0 \\ 0 & -\sqrt{2} \end{pmatrix}, \quad F^R = F^L = \begin{pmatrix} 0 & -1 \\ 1 & 0 \end{pmatrix}. \quad (16)$$

Therefore, we have

$$|\psi\rangle \equiv H|\Phi_1\rangle = \sum_{b=1}^{L_b} \sum_{\{s\}} \text{Tr}[A^{s_1} \dots F^{s_b} \dots A^{s_{L_b}}] |s_1 \dots s_{L_b}\rangle. \quad (17)$$

The norm of the above state is

$$\langle \psi | \psi \rangle = L_b \text{Tr}[E_F E_A^{L_b-1}] + L_b \sum_{m=0}^{L_b-2} \text{Tr}[E_{FA} E_A^m E_{AF} E_A^{L_b-m-2}], \quad (18)$$

where we introduced additional “transfer matrices”  $E_F \equiv \sum_s (F^s)^* \otimes F^s$ ,  $E_{FA} \equiv \sum_s (F^s)^* \otimes A^s$ , and  $E_{AF} = \sum_s (A^s)^* \otimes F^s$ . Explicitly, we have

$$E_F = 2 \begin{pmatrix} 1 & 0 & 0 & 1 \\ 0 & -1 & -1 & 0 \\ 0 & -1 & -1 & 0 \\ 1 & 0 & 0 & 1 \end{pmatrix}, \quad E_{FA} = E_{AF} = \sqrt{2} \begin{pmatrix} 0 & -1 & -1 & 0 \\ 1 & 0 & 0 & 1 \\ 1 & 0 & 0 & 1 \\ 0 & -1 & -1 & 0 \end{pmatrix}. \quad (19)$$

We then have  $\text{Tr}[E_F E_A^{L_b-1}] = 4[3^{L_b-1} + (-1)^{L_b}]$ , while  $\text{Tr}[E_{FA} E_A^m E_{AF} E_A^{L_b-m-2}] = 8(-1)^{m+1}[3^{L_b-m-2} + (-1)^{L_b} 3^m]$ , which gives us  $\sum_{m=0}^{L_b-2} \text{Tr}[E_{FA} E_A^m E_{AF} E_A^{L_b-m-2}] = -4[3^{L_b-1} + (-1)^{L_b}]$ . We thus showed that  $\langle \psi | \psi \rangle = 0$ , which means that  $H|\Phi_1\rangle = 0$ .

The fact that  $|\Phi_2\rangle$  is also an eigenstate follows from the translational invariance of the Hamiltonian:  $H|\Phi_2\rangle = HT_x|\Phi_1\rangle = T_x H|\Phi_1\rangle = 0$ .

### Relation between $|\Phi_1\rangle$ and AKLT state

It is interesting to note that there is a precise relation between our exact eigenstate  $|\Phi_1\rangle$  in the blocked representation and the celebrated AKLT state in a spin-1 chain. Specifically, we can perform the following gauge transformation  $\text{Tr}[A^{s_1} A^{s_2} A^{s_3} A^{s_4} \dots] = \text{Tr}[A^{s_1} U U^{-1} A^{s_2} A^{s_3} U U^{-1} A^{s_4} \dots] = \text{Tr}[(A')^{s_1} (A'')^{s_2} (A')^{s_3} (A'')^{s_4} \dots]$  with  $U = \sigma^x$  Pauli matrix and  $(A')^s = A^s U$ ,  $(A'')^s = U^{-1} A^s$ . The matrices  $(A')^s$  are precisely the matrices used in an MPS representation of the AKLT state with identification  $s = O, R, L$  as  $S_z = 0, 1, -1$  in the spin-1 chain, while the matrices  $(A'')^s$  become the same as  $(A')^s$  after a unitary transformation on the physical states that interchanges  $L$  and  $R$  states. Unfortunately, the Hamiltonians in the Rydberg problem and in the AKLT problem appear to be drastically different. Most notably, the Rydberg Hamiltonian has a nontrivial translation symmetry  $T_x$  by one Rydberg atom, while the AKLT Hamiltonian “knows” only about  $T_x^2$  which is the simple translation symmetry by one block in the blocked variables. Also, the AKLT Hamiltonian has continuous spin rotation symmetry and is a sum of local terms that individually annihilate the AKLT state, which is not the case for the Rydberg Hamiltonian and our exact eigenstate. So far, we have not been able to utilize knowledge about the AKLT Hamiltonian in the Rydberg problem.

### Formulas for local energies in the exact eigenstates in OBC

It is an easy exercise in MPS calculations to obtain expectation values of the local energy  $\langle X_j \rangle_{\alpha, \beta} \equiv \langle \Gamma_{\alpha, \beta} | X_j | \Gamma_{\alpha, \beta} \rangle / \langle \Gamma_{\alpha, \beta} | \Gamma_{\alpha, \beta} \rangle$  in the OBC exact eigenstates defined in Eq. (8) in the main text. The essential ingredients are generalized transfer matrices  $E_{XB} = B^0 \otimes B^1 + B^1 \otimes B^0$  and  $E_{XC} = C^0 \otimes C^1 + C^1 \otimes C^0$ , as well as ordinary transfer matrices  $E_B = B^0 \otimes B^0 + B^1 \otimes B^1$  and  $E_C = C^0 \otimes C^0 + C^1 \otimes C^1$ , where we have already used the fact that all our matrices  $B^\sigma, C^\sigma$  are real. Note that  $E_B E_C = E_A$ , which is the transfer matrix used in the blocked formulation and given in Eq. (13). We also define boundary vectors  $e_\alpha = v_\alpha \otimes v_\alpha$ , where  $\alpha = 1, 2$  (here also using that our vectors  $v_\alpha$  are real). Parameterizing our terminations as  $v_\alpha = (1, (-1)^{\alpha-1})$ ,  $\alpha = 1, 2$ , we obtain the norms as

$$\langle \Gamma_{\alpha, \beta} | \Gamma_{\alpha, \beta} \rangle = e_\alpha^T E_A^{L_b} e_\beta = 2 \left[ (-1)^{L_b + \alpha + \beta} + 3^{L_b} \right]. \quad (20)$$

For the energy calculations, at site  $j = 2b - 1$ ,  $b = 1 \dots L_b$ , we have  $\langle \Gamma_{\alpha, \beta} | X_j | \Gamma_{\alpha, \beta} \rangle = e_\alpha^T E_A^{b-1} E_{XB} E_C E_A^{L_b-b} e_\beta$ ; while at site  $j = 2b$ , we have  $\langle \Gamma_{\alpha, \beta} | X_j | \Gamma_{\alpha, \beta} \rangle = e_\alpha^T E_A^{b-1} E_B E_{XC} E_A^{L_b-b} e_\beta$ . We obtain

$$\langle X_{2b-1} \rangle_{\alpha, \beta} = \langle X_{2b} \rangle_{\alpha, \beta} = \frac{\sqrt{2}}{1 + (-1)^{L_b + \alpha + \beta} 3^{-L_b}} \left[ (-1)^\alpha (-1)^b 3^{-b} + (-1)^\beta (-1)^{L_b-b} 3^{-L_b+b-1} \right]. \quad (21)$$

These are plotted in the main text in Fig. 1. Interestingly, we can relate these states that differ by their terminations only at one edge by an action of a local two-site operator near that edge. For example,

$$|\Gamma_{1,2}\rangle = \mathbf{1}_{[1, \dots, L-2]} \otimes \left( \frac{1}{\sqrt{2}} |00\rangle \langle 01| - \frac{1}{\sqrt{2}} |00\rangle \langle 10| + |01\rangle \langle 01| - |10\rangle \langle 10| \right)_{[L-1, L]} |\Gamma_{1,1}\rangle.$$

(However, note that the operator achieving this is not unique.)

It is easy to check that the expectation value of the total energy  $\langle H \rangle_{\alpha,\beta} = \sum_{j=1}^L \langle X_j \rangle_{\alpha,\beta}$  is 0 if  $\alpha = \beta$ , while  $\langle H \rangle_{1,2} = \sqrt{2}$  and  $\langle H \rangle_{2,1} = -\sqrt{2}$ . In fact, the states are exact eigenstates and these expectation values are the corresponding eigenvalues, as we show next.

### Proof of exact eigenstates in OBC

Here we prove that  $|\Gamma_{\alpha,\beta}\rangle$  are eigenstates by showing  $\langle \Gamma_{\alpha,\beta} | H^2 | \Gamma_{\alpha,\beta} \rangle / \langle \Gamma_{\alpha,\beta} | \Gamma_{\alpha,\beta} \rangle - \langle H \rangle_{\alpha,\beta}^2 = 0$ . Here, in OBC, the Hamiltonian in the blocked form is

$$H = \sum_{b=1}^{L_b-1} h_{b,b+1} + h_{\text{left}} + h_{\text{right}}, \quad h_{\text{left}} = (|L\rangle\langle O| + |O\rangle\langle L|)_{b=1}, \quad h_{\text{right}} = (|R\rangle\langle O| + |O\rangle\langle R|)_{b=L_b}, \quad (22)$$

with the ‘‘bulk’’  $h_{b,b+1}$  given in Eq. (10).

We can write the states in the blocked representation as  $|\Gamma_{\alpha,\beta}\rangle = \sum_{\{s\}} v_{\alpha}^T A^{s_1} \dots A^{s_{L_b}} v_{\beta} |s_1 \dots s_{L_b}\rangle$ . Similar to the case in PBC, the two-body part of  $h_{b,b+1}$  annihilates these states,  $h_{b,b+1}^{(2)} |\Gamma_{\alpha,\beta}\rangle = 0$ . We therefore have

$$|\psi_{\alpha,\beta}\rangle \equiv H |\Gamma_{\alpha,\beta}\rangle = \sum_{b=1}^{L_b} \sum_{\{s\}} v_{\alpha}^T A^{s_1} \dots F^{s_b} \dots A^{s_{L_b}} v_{\beta} |s_1 \dots s_{L_b}\rangle. \quad (23)$$

Here and below, we use the same notation for appropriate MPS matrices and transfer matrices as in the PBC case. We can now calculate the squared norm:

$$\langle \psi_{\alpha,\beta} | \psi_{\alpha,\beta} \rangle = \sum_{c=2}^{L_b} \sum_{b=1}^{c-1} g_1(b, c) + \sum_{b=2}^{L_b} \sum_{c=1}^{b-1} g_2(b, c) + \sum_{b=1}^{L_b} g_3(b), \quad (24)$$

where

$$g_1(b, c) = e_{\alpha}^T E_A^{b-1} E_{FA} E_A^{c-b-1} E_{AF} E_A^{L_b-c} e_{\beta} = \frac{16}{3} \left[ (-1)^{L_b+\alpha+\beta} (-3)^{c-b} + (-3)^{b-c} 3^{L_b} \right], \quad (25)$$

$$g_2(b, c) = e_{\alpha}^T E_A^{c-1} E_{AF} E_A^{b-c-1} E_{FA} E_A^{L_b-b} e_{\beta} = \frac{16}{3} \left[ (-1)^{L_b+\alpha+\beta} (-3)^{b-c} + (-3)^{c-b} 3^{L_b} \right], \quad (26)$$

$$g_3(b) = e_{\alpha}^T E_A^{b-1} E_F E_A^{L_b-b} e_{\beta} = \frac{8}{3} \left[ 3(-1)^{L_b+\alpha+\beta} + 3^{L_b} \right]. \quad (27)$$

The summations give us

$$\begin{aligned} \sum_{c=2}^{L_b} \sum_{b=1}^{c-1} g_1(b, c) &= \sum_{b=2}^{L_b} \sum_{c=1}^{b-1} g_2(b, c) = \left[ 3^{L_b} - (-1)^{L_b} \right] \left[ 1 - (-1)^{\alpha+\beta} \right] - \frac{4}{3} \left[ 3(-1)^{L_b+\alpha+\beta} + 3^{L_b} \right] L_b, \\ \sum_{b=1}^{L_b} g_3(b) &= \frac{8}{3} \left[ 3(-1)^{L_b+\alpha+\beta} + 3^{L_b} \right] L_b, \end{aligned}$$

or  $\langle \psi_{\alpha,\beta} | \psi_{\alpha,\beta} \rangle = 2[3^{L_b} - (-1)^{L_b}][1 - (-1)^{\alpha+\beta}]$ . We therefore immediately conclude that  $H |\Gamma_{\alpha,\alpha}\rangle = 0$ ,  $\alpha = 1, 2$ . On the other hand, for  $(\alpha, \beta) = (1, 2)$  or  $(2, 1)$ , we have  $\langle \psi_{\alpha,\beta} | \psi_{\alpha,\beta} \rangle = 4[3^{L_b} - (-1)^{L_b}]$ . Recalling that  $\langle \Gamma_{1,2} | \Gamma_{1,2} \rangle = \langle \Gamma_{2,1} | \Gamma_{2,1} \rangle = 2[3^{L_b} - (-1)^{L_b}]$ , and  $\langle H \rangle_{1,2} = -\langle H \rangle_{2,1} = \sqrt{2}$ , we thereby show that  $|\Gamma_{1,2}\rangle$  and  $|\Gamma_{2,1}\rangle$  are also eigenstates with energies  $\sqrt{2}$  and  $-\sqrt{2}$  respectively.

It is interesting to note that  $\Gamma_{\alpha,\beta}$  are hence also eigenstates of a Hamiltonian containing only single-body terms in the blocked formulation,  $H' = \sum_b (|L\rangle\langle O| + |O\rangle\langle L| + |R\rangle\langle O| + |O\rangle\langle R|)_b$ , see Eq. (23) and discussion preceding Eq. (15). Each single-body term is readily solved and gives energies  $0, \pm\sqrt{2}$ . Therefore, any eigenstate of  $H'$  must have energy which is an integer multiple of  $\sqrt{2}$ . However, Eq. (23) only guarantees that  $H' |\Gamma_{\alpha,\beta}\rangle$  satisfy the Rydberg constraints and does not obviously guarantee that  $|\Gamma_{\alpha,\beta}\rangle$  are eigenstates of  $H'$ , and we needed the above detailed calculations showing zero energy variance.

### One-site and two-site reduced density matrices in PBC for finite $L_b$

Obtaining the one-site reduced density matrix of the exact states in PBC is a simple exercise in MPS calculations. For concreteness, let us consider  $|\Phi_1\rangle$ . We define generalized transfer matrices  $E_B^{\sigma\sigma'} \equiv (B^\sigma)^* \otimes B^{\sigma'}$  and  $E_C^{\sigma\sigma'} \equiv (C^\sigma)^* \otimes C^{\sigma'}$ . The ordinary transfer matrices  $E_B$  and  $E_C$  defined earlier are related to these as  $E_B = \sum_\sigma E_B^{\sigma\sigma}$  and  $E_C = \sum_\sigma E_C^{\sigma\sigma}$ . We can now obtain the matrix elements of the one-site density matrix on the odd sites as  $\langle\sigma'|\rho_{[1]}^{\text{one-site}}|\sigma\rangle = \text{Tr}[E_B^{\sigma\sigma'} E_C E_A^{L_b-1}]/\text{Tr}[E_A^{L_b}]$ . We find

$$\rho_{[1]}^{\text{one-site}} = \frac{2 \cdot 3^{L_b-1} + 1 + (-1)^{L_b}}{Z} |0\rangle\langle 0| + \frac{3^{L_b-1} + 1}{Z} |1\rangle\langle 1|, \quad Z = 3^{L_b} + 2 + (-1)^{L_b}. \quad (28)$$

On the even sites, the matrix elements are given as  $\langle\sigma'|\rho_{[2]}^{\text{one-site}}|\sigma\rangle = \text{Tr}[E_B E_C^{\sigma\sigma'} E_A^{L_b-1}]/\text{Tr}[E_A^{L_b}]$ . It is easy to verify that we indeed have  $\rho_{[1]}^{\text{one-site}} = \rho_{[2]}^{\text{one-site}}$ . For even  $L_b$ , the one-site density matrix is  $\rho_{[1]}^{\text{one-site}} = \rho_{[2]}^{\text{one-site}} = \frac{2}{3}|0\rangle\langle 0| + \frac{1}{3}|1\rangle\langle 1|$ ; while for odd  $L_b$ , it is essentially the same but with an exponentially small correction.

For the two-site reduced density matrix on sites 1 and 2, the matrix elements are given as  $\langle\sigma'_1\sigma'_2|\rho_{[1,2]}^{\text{two-site}}|\sigma_1\sigma_2\rangle = \text{Tr}[E_A^{(\sigma_1\sigma_2)(\sigma'_1\sigma'_2)} E_A^{L_b-1}]/\text{Tr}[E_A^{L_b}]$ , where  $E_A^{(\sigma_1\sigma_2)(\sigma'_1\sigma'_2)} = (A^{(\sigma_1\sigma_2)})^* \otimes A^{(\sigma'_1\sigma'_2)}$ , giving us

$$\rho_{[1,2]}^{\text{two-site}} = \frac{3^{L_b-1} + (-1)^{L_b}}{Z} |00\rangle\langle 00| + \frac{3^{L_b-1} + 1}{Z} (|01\rangle\langle 01| + |10\rangle\langle 10|) + \frac{-1 + (-1)^{L_b}}{3Z} (|01\rangle\langle 10| + |10\rangle\langle 01|). \quad (29)$$

On sites 2 and 3, the matrix elements of the two-site reduced density matrix are  $\langle\sigma'_2\sigma'_3|\rho_{[2,3]}^{\text{two-site}}|\sigma_2\sigma_3\rangle = \text{Tr}[E_B E_D^{(\sigma_2\sigma_3)(\sigma'_2\sigma'_3)} E_C E_A^{L_b-2}]/\text{Tr}[E_A^{L_b}]$ , where  $E_D^{(\sigma_2\sigma_3)(\sigma'_2\sigma'_3)} \equiv (C^{\sigma_2} B^{\sigma_3})^* \otimes (C^{\sigma'_2} B^{\sigma'_3})$ . We find

$$\rho_{[2,3]}^{\text{two-site}} = \frac{3^{L_b-1} + (-1)^{L_b}}{Z} |00\rangle\langle 00| + \frac{3^{L_b-1} + 1}{Z} (|01\rangle\langle 01| + |10\rangle\langle 10|) + \frac{1 - 3^{L_b-2}}{Z} (|01\rangle\langle 10| + |10\rangle\langle 01|). \quad (30)$$

For large  $L_b$ , these reduce to expressions Eqs. (6) and (7) in the main text.

### Entanglement spectra of exact eigenstates in OBC

To obtain the entanglement spectrum for the states  $|\Gamma_{\alpha,\beta}\rangle$ , we follow the procedure in Refs. [13, 18]. First, we consider the entanglement cut between the sites  $2b$  and  $2b+1$ . We form  $2 \times 2$  Gram matrix  $\mathcal{L}_{2 \times 2}$  reshaped from  $e_\alpha^T E_A^b$  and  $2 \times 2$  Gram matrix  $\mathcal{R}_{2 \times 2}$  reshaped from  $E_A^{L_b-b} e_\beta$ , and then obtain an effective matrix

$$\mathcal{S}_{2 \times 2} = \frac{\mathcal{L}_{2 \times 2} \mathcal{R}_{2 \times 2}}{\langle \Gamma_{\alpha,\beta} | \Gamma_{\alpha,\beta} \rangle} = \frac{1}{2} \begin{pmatrix} 1 & \frac{(-1)^{\alpha+1} 3^{L_b-b} + (-1)^{\beta+1} 3^b}{(-1)^{L_b+\alpha+\beta+3L_b}} \\ \frac{(-1)^{\alpha+1} 3^{L_b-b} + (-1)^{\beta+1} 3^b}{(-1)^{L_b+\alpha+\beta+3L_b}} & 1 \end{pmatrix} \quad (31)$$

whose eigenvalues are the same as eigenvalues of the reduced density matrix. We therefore obtain the entanglement spectrum as

$$s_{1,2} = \frac{1}{2} \left( 1 \pm \frac{(-1)^{\alpha+1} 3^{L_b-b} + (-1)^{\beta+1} 3^b}{(-1)^{L_b+\alpha+\beta+3L_b}} \right). \quad (32)$$

For large subsystem size  $b$  and in the thermodynamic limit, e.g., where we take  $L_b \rightarrow \infty$ ,  $b \rightarrow \infty$ , while fixing the ratio  $b/L_b = f < 1$ , or where we take  $L_b \rightarrow \infty$  first and then  $b \rightarrow \infty$ , the entanglement spectrum approaches  $s_{1,2} \rightarrow 1/2$  independent of the terminations.

For the entanglement cut between sites  $2b+1$  and  $2b+2$ , we need  $3 \times 3$  Gram matrix  $\mathcal{L}_{3 \times 3}$  reshaped from  $e_\alpha^T E_A^b E_B$  and  $3 \times 3$  Gram matrix  $\mathcal{R}_{3 \times 3}$  reshaped from  $E_C E_A^{L_b-b-1} e_\beta$ . The effective matrix that reproduces the entanglement spectrum is

$$\mathcal{S}_{3 \times 3} = \frac{\mathcal{L}_{3 \times 3} \mathcal{R}_{3 \times 3}}{\langle \Gamma_{\alpha,\beta} | \Gamma_{\alpha,\beta} \rangle} = \frac{1}{3^{L_b} + (-1)^{L_b+\alpha+\beta}} \begin{pmatrix} \frac{5}{6} \cdot 3^{L_b} + \frac{1}{2} \cdot (-1)^{L_b+\alpha+\beta} & \frac{1}{6} \cdot (-1)^{1+b} [(-1)^\alpha \cdot 3^{L_b-b} + 9 \cdot (-1)^{L_b+\beta} \cdot 3^b] & -3^{L_b-1} \\ \frac{1}{2} \cdot (-1)^{1+b} [(-1)^\alpha \cdot 3^{L_b-b} + (-1)^{L_b+\beta} \cdot 3^b] & \frac{1}{6} \cdot 3^{L_b} + \frac{1}{2} \cdot (-1)^{L_b+\alpha+\beta} & (-1)^{b+\alpha} \cdot 3^{L_b-b-1} \\ 3^{L_b-1} & (-1)^{1+\beta+L_b-b} \cdot 3^b & 0 \end{pmatrix}. \quad (33)$$

The entanglement spectrum at any finite  $L_b$ ,  $b$  can be obtained from the eigenvalues of the above matrix. For large  $b$  and in the thermodynamic limit, we have

$$\mathcal{S} \rightarrow \begin{pmatrix} \frac{5}{6} & 0 & -\frac{1}{3} \\ 0 & \frac{1}{6} & 0 \\ \frac{1}{3} & 0 & 0 \end{pmatrix}, \quad (34)$$

which gives the entanglement spectrum  $2/3$ ,  $1/6$  and  $1/6$  quoted in the main text.

---